Data Repository Item

Appendix DR1

Materials and methods

Dating

Samples 360-5 to 360-19 were processed by Donelick Analytical and analyzed by A. Blythe (set 1), all other samples were processed by Alexander Grist at Dalhousie University and analyzed by I. Coutand (set 2): standard magnetic and heavy liquid mineral separation procedures were used. Apatites were mounted in araldite epoxy. Sample surfaces were ground and polished. Apatite mounts were etched in 7% HNO_3 at 18°C for 22s (set 1) and etched in 5M HNO_3 at 24°C for 20s (set 2). An "external detector" (Naeser, 1979), consisting of low-U (<5 ppb) muscovite, was used for each sample. Samples were irradiated in the Cornell University Triga nuclear reactor (set 1) and at the Dalhousie University Slowpoke reactor (set 2). Following irradiation, the muscovites were etched in 48% HF for 30 min at 18°C (set 1) or room temperature (set 2). Tracks were counted using a 100X dry lens and 1250X total magnification in crystals with well-etched, clearly visible tracks and sharp polishing scratches. A Kinetek stage and software (Dumitru, 1993) were used for analyses. Standard and induced track densities were determined on external detectors (geometry factor = 0.5), and spontaneous track densities were determined on internal mineral surfaces. Ages were calculated using $\zeta = 320 \pm 9$ for dosimeter glass SRM 962a for A. Blythe and $\zeta = 369.5 \pm 5.1$ for dosimeter glass CN5 for I. Coutand.

Long-term erosion rate

Apatite fission-track ages are interpreted to indicate the time elapsed since cooling below the effective closure temperature of the system. This temperature is dependent on the kinetic characteristics of the apatite crystal and the cooling rate (Ketcham et al., 1999). If the depth of the closure isotherm (which is dependent on the geothermal gradient) can be estimated, then AFT ages can be converted into mean exhumation (or erosion) rates (Stüwe et al., 1994; Brandon et al., 1998; Willett and Brandon, 2002). In our samples, Dpar measurements corrected from Donelick et al. (1999), indicate mostly kinematically homogeneous apatite crystals with a low resistance to annealing and an effective closure T of 120 ± 20°C for cooling rates between 10-100°C/Ma (Ketcham et al., 1999).

Samples were collected at elevations below ~ 4000 m, excluding areas that were recently glaciated. With this sampling strategy, lithological and structural influence on erosion is minimized and the mixture of glacial and fluvial erosion processes avoided. Sampling along transects across valleys (rather than along valleys) over a distance five times longer than the wavelength of the surface topography (typical spacing between the valley bottoms along the studied transect) provides the mean regional exhumation rates at a time defined by the mean age of rocks for the AFT thermochronometer (Braun, 2002).

We extracted erosion rates, fully aware of the perturbations of the near surface isotherms in active orogens with high relief and heat flow and the effects of non-steady landscape (Stüwe et al., 1994; Mancktelow and Grasemann, 1997; Stüwe and Hintermüller, 2000; Braun, 2002). In order to extract long-term exhumation rates, we calculated the

weighted mean AFT ages for each area, assumed a steady exhumation with T_{surf}= 10°C, T_c=120 ± 20°C and dT/dz (geothermal gradient)= 30-40°C/km. Similar exhumation rates were obtained using the program AGE2DOT (Brandon et al., 1998). For a short transect at the Trumshing La, we extracted the apparent exhumation rate from the relationship of AFT ages vs. corresponding elevation (age elevation relationship, AER). The regression line was fit using weighted least squares (Brandon et al., 1998; Press et al., 1992, p. 655-660). Errors were assumed to reside totally in the fission-track ages and weights were assigned using the age uncertainties. The estimated exhumation rate is equal to the slope of the regression line and its errors are calculated from the uncertainty for the estimated regression slope.

Precipitation map

The precipitation map is based on measurements derived from the TRMM (Tropical Rainfall Measurement Mission) satellite (Bookhagen et al., 2005). The TRMM has a high spatial (~5x5km) and temporal resolution that allows constructions of a rainfall map on the presented scale. We calibrated precipitation for the Indian Summer Monsoon for the last 7 years from 1998 to 2004 by using the meteorological stations of Department of Energy, MTI, Thimphu, Bhutan (Royal Government of Bhutan 2003 report). The processed TRMM data are within 10% range of the station data. However, the satellite-derived rainfall amounts can capture the synoptic scale moisture transport much better than a limited number of ground stations.

DEM

The digital elevation model (DEM) was produced from the 3 arc-second resolution Shuttle Radar Topography Mission (SRTM) data. The effective resolution is roughly 80 x 93 m at the latitude of Bhutan. The original data were patched with edge-matched, IDW edge-difference interpolated 3 arc-second DTED data. The patched data were then projected onto a 75-m equal area grid.

Remnants of the low-relief relict landscape were contoured by superposition of slope and elevation maps. As proxy for the slope we used local relief that was computed as standard deviation of DEM elevations within a 5-cell (375 m) radius moving window.

Table DR1 Apatite fission-track data

N, number of individual grains dated; ρ_s, spontaneous track density; Ns, number of spontaneous tracks counted; ρ_i, induced track density in external detector (muscovite); Ni, number of induced tracks counted; ρ_d, induced track density in external detector adjacent to dosimetry glass; Nd, number of tracks counted in determining ρ_d; P(χ^2), chi-square probability; Trackkey software (Dunkl, 2002) was used to calculate the central fission-track ages. Analytical precisions of 0.3 to 1.5 Ma ($\pm 1\sigma$) could be obtained from these young AFT ages due to the high U-content and the number of grains counted per sample. Note that zero-track grains were considered. Set 1 counted by I. Coutand, set 2 counted by A. Blythe. The samples are arranged with their increasing longitude from west to east.

Table DR1 Apatite fission-track data

Set	Field code	Longitude	Latitude	Elevation	Number of grains	Spontaneous track density	Induced track density	Dosimeter	$P(\chi^2)$	Central age ± 1σ
		[° E]	[° N]	[km]		$\rho s \times 10^5$ cm^{-2}	$\rho i \times 10^5$ cm^{-2}	$\rho d \times 10^5$ cm^{-2}	[%]	[Ma]
					(N)	(Ns)	(Ni)	(Nd)		
1	BH299	89.33608	27.79572	4.729	25	0.453 (99)	17.06 (3725)	9.7284 (7938)	89.27	4.4 ± 0.5
1	BH109	89.399720	27.442220	2.400	22	1.265 (246)	37.541 (7303)	9.7661 (7938)	78.55	6.1 ± 0.4
2	F01a	89.409061	26.862184	0.644	20	0.196 (9)	26.621 (1225)	13.5 (2201)	88	1.8 ± 0.6
2	F04	89.459331	26.907234	1.751	13	0.077 (5)	13.057 (844)	13.1 (2085)	58	1.4 ± 0.6
2	F07	89.552425	27.189091	2.153	20	0.446 (38)	44.243 (3766)	21.4 (3424)	98	3.5 ± 0.6
2	F06	89.557211	27.065828	1.545	20	0.523 (67)	27.539 (3525)	21.4 (3424)	99	6.5 ± 0.8
2	F05	89.574151	27.027370	1.881	20	0.609 (78)	31.383 (4017)	21.7 (3477)	32	6.7 ± 0.8
2	F17	89.695204	27.441718	2.524	20	0.313 (23)	37.785 (2781)	19.7 (3162)	95	2.6 ± 0.6
2	F08	89.748838	27.490287	3.113	20	0.423 (42)	23.337 (2315)	12.7 (1999)	68	4.1 ± 0.7
1	BH171	89.770810	27.692940	1.440	23	0.13 (24)	10.113 (1868)	9.7472 (7938)	97.72	2.3 ± 0.5
2	F09	89.796000	27.512400	1.953	20	0.316 (26)	29.027 (2389)	21.1 (3372)	92	3.7 ± 0.7
2	F14	89.906482	27.450639	1.192	20	0.175 (16)	20.07 (1832)	20.1 (3215)	97	2.8 ± 0.7
2	F10	89.911594	27.363505	1.044	20	0.367 (47)	31.680 (4055)	20.7 (3320)	96	3.8 ± 0.6
2	F16	89.962020	27.506429	1.399	20	0.256 (23)	36.819 (3299)	20.1 (3215)	74	2.2 ± 0.5
2	F13	89.986095	27.290790	0.881	29	0.062 (8)	14.193 (1844)	20.4 (3268)	47	1.4 ± 0.5
2	F13b	89.986095	27.290790	0.881	20	0.166 (8)	12.720 (613)	19.7 (3162)	78	4.1 ± 1.5
2	F11	90.036966	27.263110	0.71	20	0.497 (31)	31.282 (1950)	20.7 (3320)	78	5.3 ± 1.0
2	F12	90.076180	27.032043	0.361	20	0.214 (22)	35.278 (3635)	20.4 (3268)	99	2.0 ± 0.4
1	BH347	90.299306	27.524611	2.590	19	0.297 (41)	7.898 (1090)	9.9922 (7938)	69.73	6.9 ± 1.1
1	BH346	90.432250	27.447417	2.390	24	0.931 (171)	26.502 (4869)	9.7849 (7938)	36.35	6.3 ± 0.5
1	BH344	90.468250	27.507806	1.920	21	1.146 (222)	34.893 (6757)	10.011 (7938)	89.81	6.1 ± 0.4

1	BH345	90.481361	27.473000	2.220	24	0.916 (210)	27.276 (6250)	9.9545 (7938)	99.13	6.2 ± 0.4
1	BH104	90.996972	27.399139	3.710	25	0.513 (123)	11.445 (2745)	10.399 (7383)	49.27	8.6 ± 0.8
1	BH103	91.006333	27.399139	3.300	24	0.672 (147)	16.748 (3663)	10.517 (7383)	77.35	7.8 ± 0.7
1	BH102	91.055167	27.329000	2.795	19	1.114 (148)	32.919 (4375)	10.428 (7383)	87.51	6.5 ± 0.6
1	BH101	91.100722	27.341333	2.380	39	0.42 (129)	13.106 (4022)	10.31 (7383)	90.36	6.1 ± 0.6
1	BH100/2	91.153889	27.308806	1.720	24	0.115 (26)	3.667 (829)	10.25 (7383)	97.47	5.9 ± 1.2
1	BH60	91.480667	27.282361	0.795	24	0.3 (67)	14.946 (3341)	11.356 (8092)	85.85	4.2 ± 0.5
1	BH61	91.491000	27.303417	0.780	25	0.943 (159)	37.117 (6261)	11.397 (8092)	73.63	5.4 ± 0.4
1	BH70	91.499528	27.584167	1.760	19	1.593 (230)	82.415 (11901)	10.369 (7383)	91.29	3.7 ± 0.3
1	BH53	91.548083	27.237361	2.405	25	0.219 (30)	6.655 (910)	11.315 (8092)	86.74	6.9 ± 1.3
1	BH64	91.554472	27.350056	0.825	25	0.133 (28)	9.198 (1933)	11.353 (8092)	33.48	3.0 ± 0.7
1	BH52	91.554667	27.236056	2.350	26	0.259 (42)	7.752 (1255)	11.288 (8092)	70.3	7.8 ± 1.4
1	BH72	91.554722	27.465000	1.420	24	1.208 (269)	42.927 (9562)	10.547 (7383)	56.04	5.5 ± 0.4
1	BH66	91.561139	27.551361	0.930	22	0.345 (55)	14.78 (2358)	10.28 (7383)	92.34	4.4 ± 0.6
1	BH100	91.563722	27.411389	0.905	21	1.203 (241)	43.357 (8686)	11.465 (8092)	75.2	5.9 ± 0.4
1	BH90	91.574528	27.344972	0.910	25	0.258 (45)	14.916 (2604)	11.302 (8092)	70.26	3.6 ± 0.5
1	BH324	91.596833	27.374361	1.995	20	0.623 (101)	23.949 (3882)	9.9168 (7938)	91.05	4.8 ± 0.5
1	BH94	91.599833	27.375333	2.050	20	2.424 (397)	77.921 (12761)	11.533 (8092)	70.82	6.6 ± 0.4
1	BH74	91.687556	27.362556	1.415	23	0.429 (46)	19.535 (2095)	11.37 (8092)	90.96	4.6 ± 0.7
1	BH75	91.687556	27.362556	1.415	20	0.83 (122)	48.197 (7083)	11.383 (8092)	72.56	3.6 ± 0.3
1	BH329	91.792417	27.311806	3.050	22	0.375 (52)	13.718 (1904)	10.03 (7938)	83.5	5.1 ± 0.7
1	BH337	91.892722	27.415528	2.645	24	0.519 (96)	26.951 (4986)	9.8603 (7938)	85.76	3.5 ± 0.4
1	BH334	91.919389	27.384417	2.890	25	0.455 (98)	21.34 (4594)	9.8226 (7938)	98.8	3.9 ± 0.4
1	BH333	91.923700	27.275040	4.160	18	1.132 (166)	27.696 (4062)	9.898 (7938)	59.27	7.5 ± 0.6

References DR

Bookhagen, B., C., T.R., and Strecker, M.R., 2005, Abnormal Monsoon Years (AMYs) and their control on erosion and sediment flux in the high, arid northwest Himalaya: Earth and Planetary Science Letters, v. 231, p. 131-146.

Brandon, M.T., Roden-Tice, M.R., and Garver, J.I., 1998, Late Cenozoic exhumation of the Cascadia accretionary wedge in the Olympic Mountains, northwest Washington State: GSA Bulletin, v. 110, p. 985-1009.

Braun, J., 2002, Quantifying the effect of recent relief changes on age-elevation relationships: Earth and Planetary Science Letters, v. 200, p. 331-343.

Dumitru, T.A., 1993, A new computer-automated microscope stage system for fission-track analysis: Nuclear Tracks and Radiation Measurements, v. 21, p. 575-580.

Dunkl, I., 2002, Trackkey: a windows program for calculation and graphical presentation of fission track data: Computers & Geosciences, v. 28, p. 3-12.

Donelick, R.A., Ketcham, R.A., and Carlson, W.D., 1999, Variability of apatite fission-track annealing kinetics; II, Crystallographic orientation effects: American Mineralogist, v. 84, p. 1224-1234.

Ketcham, R.A., Donelick, R.A., and Carlson, W.D., 1999, Variability of apatite fission-track annealing kinetics; III, Extrapolation to geological time scales: American Mineralogist, v. 84, p. 1235-1255.

Mancktelow, N.S., and Grasemann, B., 1997, Time-dependent effects of heat advection and topography on cooling histories during erosion: Earth and Planetary Science Letters, v. 270, p. 167-195.

Naeser, C.W., 1979, Fission-track dating and geologic annealing of fission tracks, in Jäger, E., and Hunziker, J.C., eds., Lectures in isotope geology: Berlin, Federal Republic of Germany (DEU), Springer Verlag, p. 154-169.

Press, W. H., Teukolsky, S. A., Vetterling, W. T., and Flannery, B. P., 1992, Numerical recipes in Fortran: The art of scientific computing: Cambridge, Cambridge University Press, 963 p.

Stüwe, K., and Hintermüller, M., 2000, Topography and isotherms revisited: the influence of laterally migrating drainage divides: Earth and Planetary Science Letters, v. 184, p. 287-303.

Stüwe, K., White, L., and Brown, R., 1994, The influence of eroding topography on steady-state isotherms. Application to fission track analysis: Earth and Planetary Science Letters, v. 124, p. 63-74.

Willett, S.D., and Brandon, M.T., 2002, On steady states in mountain belts: Geology, v. 30, p. 175-178.

Figure Captions

Figure DR1. Precipitation map of Bhutan and Shillong Plateau plotted on the topography derived from SRTM data. The orographic barrier of the Shillong Plateau induces a decrease in precipitation along the southern Himalayan front between 90.5°E and 92°E.

Figure DR2. Histograms indicate the frequency *f* and percentage % of age bins for the corresponding data sets. In both histograms the percentage of ages for the whole of Bhutan is indicated by the grey bars.

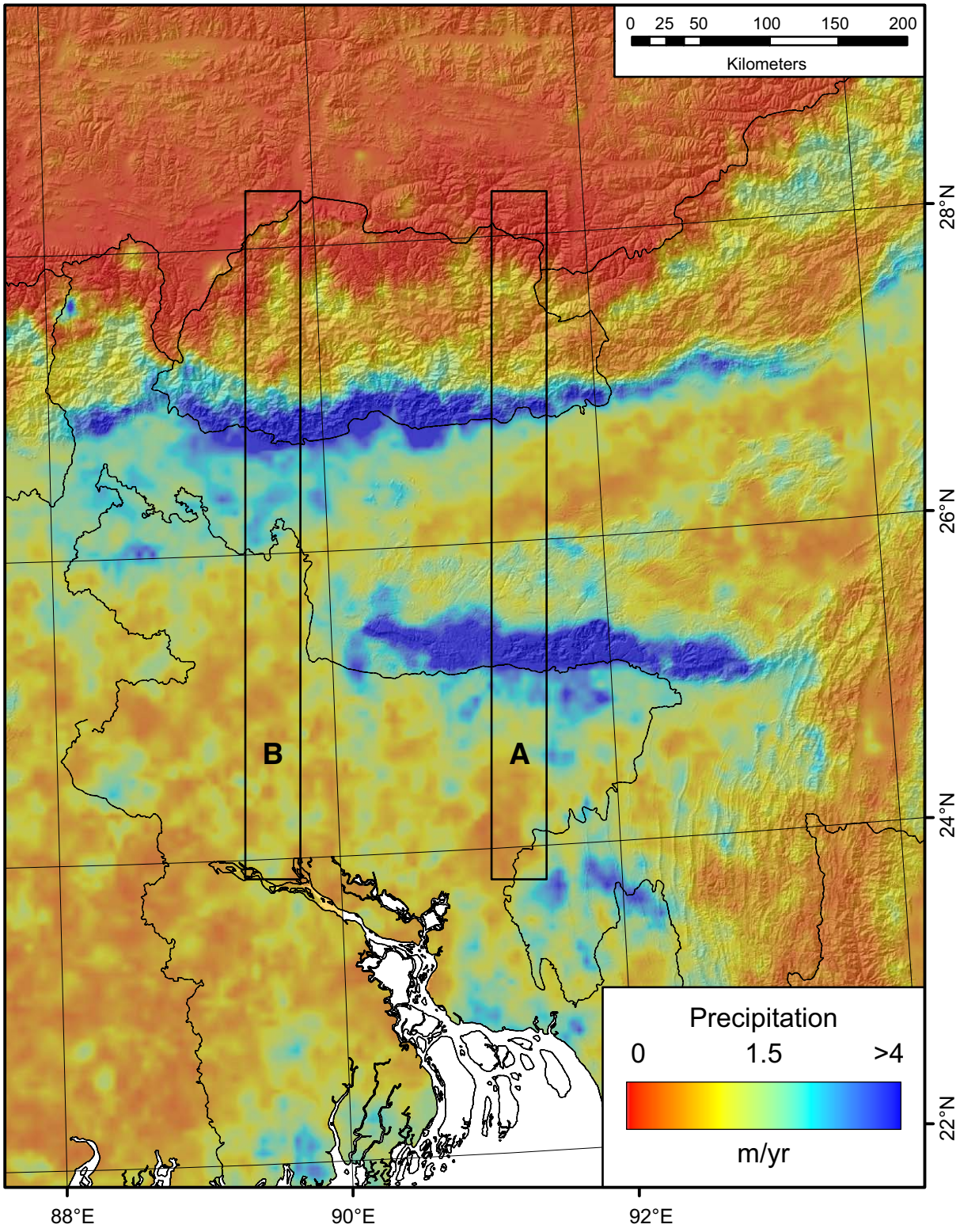

Data repository Material Figure 1

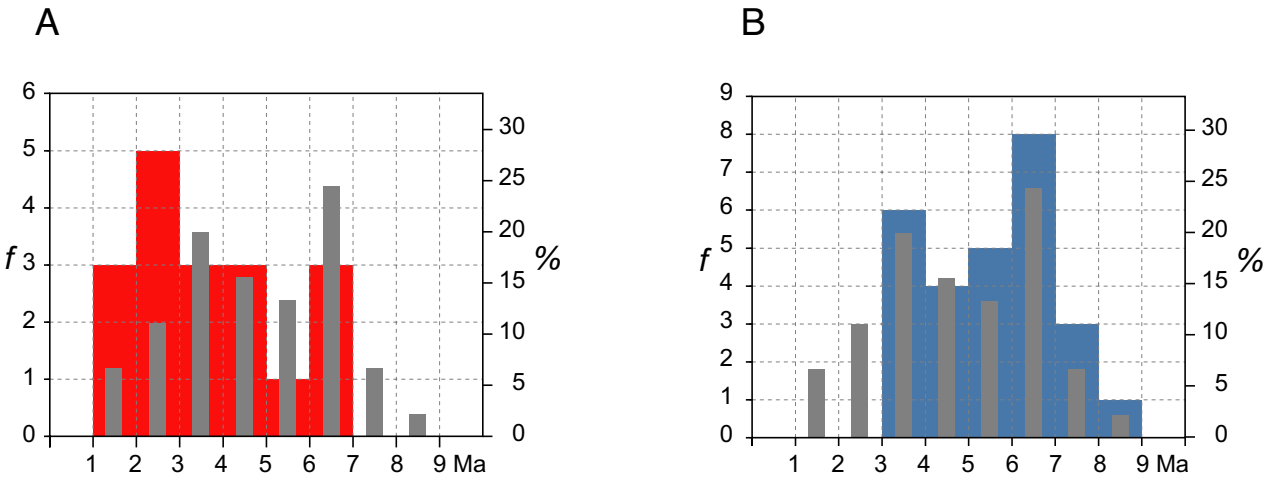

Figure DR2